Evolution of Relationships Between Dislocation Microstructures and Internal Stresses of AISI 316L During Cyclic Loading at 293 K and 573 K (20 °C and 300 °C)

MINH-SON PHAM and STUART R. HOLDSWORTH

The evolution of dislocation densities and of dislocation microstructures during cyclic loading of AISI 316L is systematically evaluated. In addition, internal stresses are also measured for every cycle and comprehensively analyzed. These observations are made in order to establish relationships between the evolution of dislocation condition and internal stresses, and ultimately to obtain a thorough insight into the complex cyclic response of AISI 316L. Moreover, the dependencies of established relationships on the variation of temperature and strain amplitude are investigated. The back stresses (long-range stresses associated with the presence of collective dislocations over different length scales) are mainly responsible for the cyclic deformation response at high strain amplitudes where dislocations tend to move more quickly in a wavy manner. In contrast, the effective stress, coupling with short-range dislocation interactions, plays an insignificant role on the material cyclic response for wavy slip conditions, but increasingly becomes more important for planar slip conditions. The additionally strong short-range interactions between dislocations and point defects (initially with solute atoms and later in life with corduroy structure) at 573 K (300 °C) cause dislocations to move in more planar ways, resulting in a significant increase in effective stress, leading to their influential role on the material cyclic response.

DOI: 10.1007/s11661-013-1981-7

I. INTRODUCTION

POLYCRYSTALLINE materials usually exhibit complex cyclic deformation responses due to their changing dislocation condition, in particular those whose dislocations first tend to move in a more planar manner during fatigue loading because the movement character can change into a more wavy form upon further loading.[1–4] For example, significant changes in the density and the configuration of dislocations during fatigue loading are responsible for the complex cyclic deformation response of AISI 316L, *e.g.*, cyclic hardening, softening in general,[5–8] or even serrated flow stress and secondary cyclic hardening after a high number of cycles at elevated temperatures.[9–11] Moreover, changes in imposed strain amplitude also lead to variations in dislocation evolution characteristics, resulting in different material responses. These cause difficulties to understand and ultimately to model the cyclic deformation response of polycrystalline materials.[12] Since effective and back stresses, respectively, are associated with the short-range and long-range order of dislocation interactions,[13–17] the variation of microstructural condition causes the change in associated internal stresses (*i.e.*, effective stress and back stresses). For example, individual dislocations can interact with themselves and with point defects thanks to their associated short-range stress fields, resulting in a change in the local resistance to dislocation movement, in particular for face-centered cubic materials.[18] The change in local resistance to dislocation movement correlates with the effective stress (σ_E) which is responsible for the expansion (or the contraction) of the yield surface in principal stress coordinates.[15] In contrast, back stress (X) is associated with long-range interactions of collective dislocations, which arise due to inhomogeneous plastic deformation between microstructural heterogeneities of materials on different scales, *e.g.*, grains, sub-grains, cell blocks, and families of dislocation walls/channels.[5,18–23] Consequently, investigation of the evolution of the microstructural condition and associated internal stresses as well as their relationships during cyclic loading provides a thorough understanding of the cyclic deformation response of metallic materials. There have been a number of studies concerning the relationship between internal stresses and dislocation conditions.[13–15,19,24–27] Most of these concentrate on the links between internal stresses and well-organized wall/channel dislocation structures. Interestingly, there is not much information

MINH-SON PHAM, Research Associate, formerly with the EMPA: High Temperature Integrity Group, Mechanics for Modelling and Simulation, Swiss Federal Laboratories for Materials Science & Technology, 8600 Dübendorf, Switzerland, and also with the Center of Mechanics, Department of Mechanical Engineering and Processing, Swiss Federal Institute of Technology Zurich (ETHZ), Zurich, Switzerland, is now with the Materials Science and Engineering Department, Carnegie Mellon University, Pittsburgh PA. Contact e-mail: minhson@andrew.cmu.edu STUART R. HOLDSWORTH, Group Leader, is with the EMPA: High Temperature Integrity Group, Mechanics for Modelling and Simulation, Swiss Federal Laboratories for Materials Science & Technology.

Manuscript submitted April 15, 2013.
Article published online September 6, 2013

concerning the evolution of this relationship which is essential to develop an effective evolutionary constitutive model in order to accurately simulate the cyclic deformation response. One of the main objectives of this present study is to understand the evolution of the relationship between internal stresses and the corresponding microstructure during cyclic loading.

The material examined in this study is AISI 316L steel which exhibits a complex cyclic deformation response which is associated with the development of the dislocation condition during cyclic loading.[6–8,10,11,28–30] In addition, this material is widely used in engineering, for example, in the pipe-cooling circuits of light-water nuclear power plants for which the working temperature is about 573 K (300 °C). Understanding the cyclic deformation behavior of the material under such conditions is essential to verify the safety factors applied to the material in service duty. Most previous studies concerning the cyclic deformation response of this material concentrated on the microstructural condition either after a high number of cycles or at failure.[6–8,10,11,28–30] In general, if a well-annealed austenitic stainless steel is cyclically strained at low plastic strain amplitudes, the dislocation structure is present in the form of planar arrangements (associated with stacking faults, pile-ups, *etc*.) until failure, which is almost similar to the initial condition, except the dislocation density is higher at the end of life. At intermediate plastic strain amplitudes, persistent slip bands and veins coexisting with dislocation-free regions (*i.e*., channels) are observed at failure. At high plastic strain amplitudes, well-organized structures, namely, wall/channel or cellular structures, are observed at failure. Our recent studies on this topic provide a detailed description of microstructural evolution during different cyclic deformation response stages and lead to a deeper insight into the relationship between microstructural condition and material deformation/damage responses.[5,9,12,31,32] In order to obtain a thorough understanding of how the material behaves during cyclic deformation as well as to provide a basis for the further development of an effective constitutive model for accurately describing the material cyclic response, it is necessary to establish the links between internal stresses and the development of microstructures. This study therefore aims to understand the evolution of this relationship at both 293 K and 573 K (20 °C and 300 °C) by exhaustively examining the evolution of microstructural features and evaluating internal stresses of AISI 316L during cyclic loading at these temperatures. The amplitude and slip-character dependencies of the relationships are also examined. In this study, systematic observations and quantifications of the microstructural condition in samples fatigued to selected numbers of cycles in the different stages of cyclic mechanical response over a range of strain amplitudes at 293 K and 573 K (20 °C and 300 °C) are made in order to quantify dislocation densities and the dimensions of dislocation microstructures. In addition, the changes in internal stresses during cyclic loading are measured from hysteresis loops according to the method of Cottrell.[18,23] The evolution of internal stresses is analyzed and then related to the dislocation condition. Thereby, the history and amplitude dependence of the roles of internal stresses on the material mechanical response at 293 K and 573 K (20 °C and 300 °C) are revealed. Finally, the detailed relationships between microstructural condition and the material deformation response are established and discussed.

II. EXPERIMENTAL PROCEDURES

The composition of the studied AISI 316L steel is shown in Table I. The material originated from a hot-finished pipe which had been quenched in water from 1323 K to 1353 K (1050 °C to 1080 °C). The inner and outer diameters of the pipe were 173 and 220 mm, respectively.

Cylindrical test pieces, with a parallel length of 20 mm, a gage diameter of 8 mm, and with threaded M16 end grips, were machined from the pipe with an axial orientation, in accordance with the requirement of ISO 12106. The test pieces were fatigue loaded with constant total strain amplitudes of ±0.7, ±0.4, and ±0.25 pct, at a strain rate of 10^{-3} 1/s, and at 293 K and 573 K (20 °C and 300 °C) using a servo-controlled electromechanical 50-kN machine. A Class-0.5 side-entry contacting extensometer with a gage length of 15 mm was attached to the test piece parallel length to control and measure strain during cyclic loading.

Recorded data were analyzed by Matlab-based subroutines. For every cycle, the subroutines determined the following: effective stress, back stress, maximum stress, and the rate of change of these stresses at different stages of mechanical response (Figures 1(a) and (b)). In this study, the approach for determining effective stress and back stress was adopted from the method of Cottrell.[18,23] Figure 1 shows a scheme for the quantitative measurement of such parameters from a stress–strain hysteresis loop. σ_0 was measured as the offset yield strength corresponding to a plastic strain of 0.05 pct. Although this definition of σ_0 took a small account of back stress, this offset strength was used in order to make a non-subjective indication of change of effective stress, in particular for low strain amplitude conditions. This helped to quantify the rate of change of this internal stress with high confidence. The cyclic deformation response rates were determined as slopes of the most linear parts during the different $\sigma_{max}(\log N)$ response stages. Positive rate values represented cyclic hardening response, whereas negative values represented cyclic softening response.

Tested specimens were sectioned parallel to the loading axis using a diamond cutting machine in order to prepare samples for microstructural observation. The samples were mechanically polished to produce thin plates of 0.1 mm thickness which were then punched out to produce disks having a diameter of 3 mm. These were marked to indicate the loading direction (LD). The disks were then electrolytically polished using a double jet device (TenuPol5) with an electrolyte solution of acetic acid and perchloric acid to provide specimens for TEM investigation. Thereafter, samples were observed in a Philips CM30 transmission electron microscope at 300 kV with a double tilt holder. The mark of the LD

Table I. Material Composition

C (Pct)	Mn (Pct)	P (Pct)	S (Pct)	Cr (Pct)	Mo (Pct)	Ni (Pct)	Cu (Pct)	B (Pct)	Co (Pct)	N (Pct)
0.014	1.630	0.030	0.002	16.730	2.120	11.090	0.600	0.0011	0.090	0.060

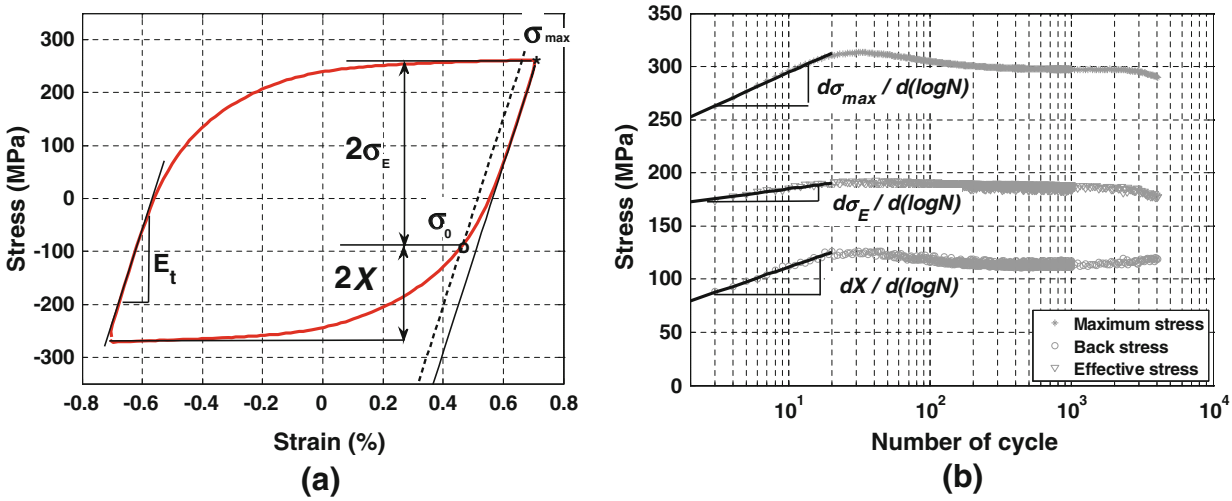

Fig. 1—(*a*) Scheme for quantitative measurement of effective and back stresses (σ_0 is the offset yield strength corresponding to a plastic strain of 0.05 pct). (*b*) Representation of the fitting procedure to measure the rates of change of cyclic hardening/softening.

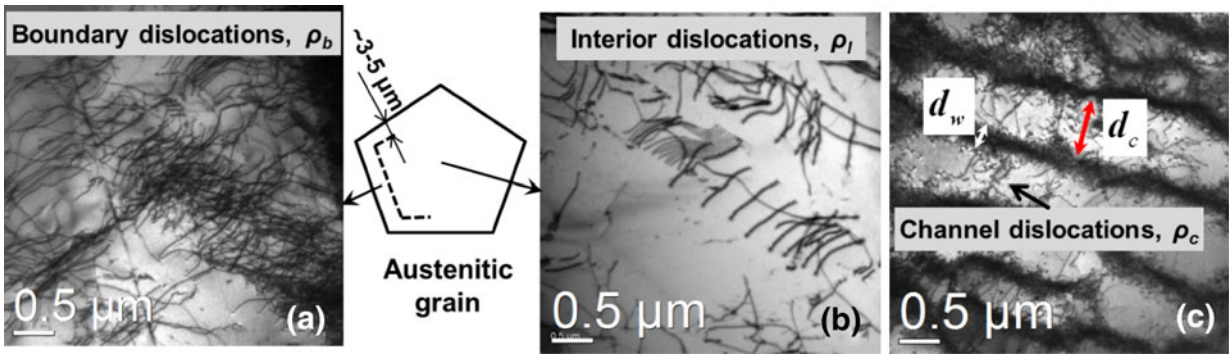

Fig. 2—Scheme of the quantitative measurement of dislocation densities in regions: (*a*) close to grain boundaries (which are hereafter called boundary dislocations), (*b*) inside grains (which are called interior dislocations). (*c*) Parameters for representing dislocation walls and channels.

was aligned along the holder axis in order to preserve the LD during observations.

Dislocation density was measured from TEM images using a point intersection method which is explained in detail elsewhere.[5] Different dislocation features representing the microstructural condition during cyclic loading were measured as described in Figure 2. During the first cycles, dislocations usually pile up against grain boundaries, whereas the number of dislocations within grain interiors is much lower.[20,33] In this study, dislocations in regions close to grain boundaries are named boundary dislocations (ρ_b), while ones present within the grains are referred to as interior dislocations (ρ_I) (Figures 2(a) and (b)). This gradient in dislocation distribution (explained in detail later in the paper) is due to the requirement to accommodate plastic strain incompatibilities between grains during plastic deformation. This indicates that dislocations close to grain boundaries at an early stage of cyclic plastic deformation are mainly of the "necessary" type. It is therefore important to differentiate and quantify the evolution of two kinds of dislocation populations. The changes in density of these two dislocation groups are quantified in an attempt to reveal their individual contributions to material response. The areas occupied by boundary dislocations were experimentally found during TEM observation to be about 10 pct (with the corresponding width of these regions at grain boundaries approximately varying between 3 and 5 μm). Once dislocation structures formed, the dislocation density within channels and the dimensions of dislocation walls were quantified (Figure 2(c)). There were three thin foils examined for each tested condition. The quantification of dislocation features was done for several grains for

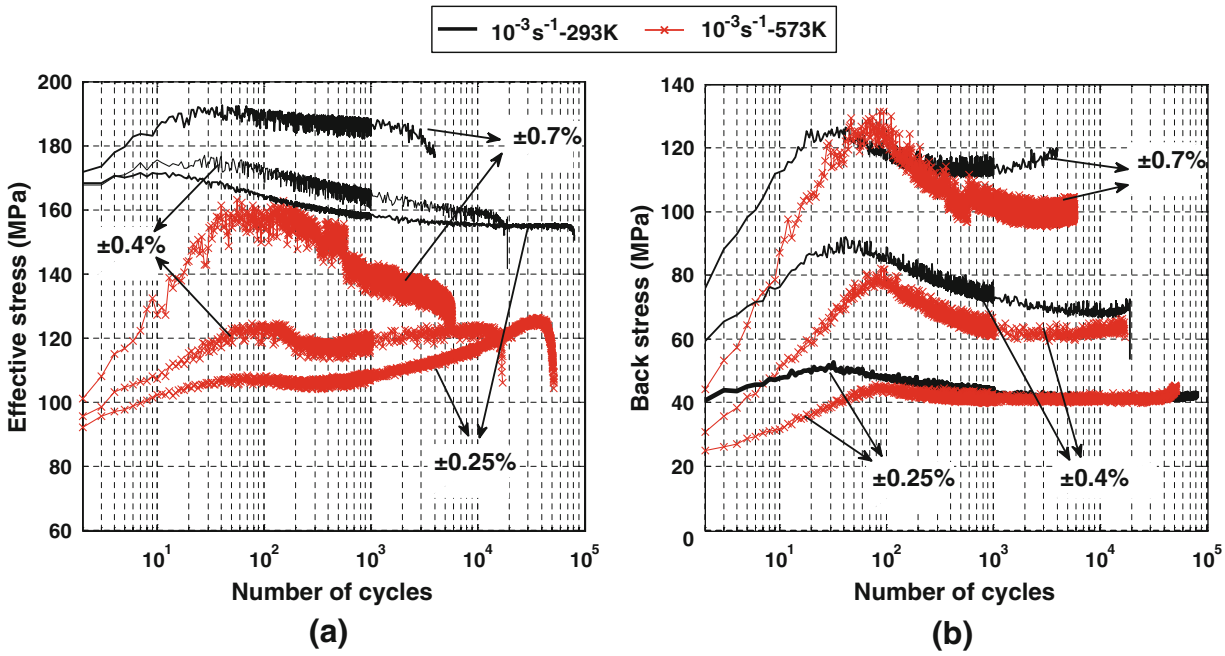

Fig. 3—Effective stress and back stress variations during cyclic loading at 293 K (20 °C) (non-marked lines) and at 573 K (300 °C) (marked lines). (*Note*: the back stress for the ±0.7 pct–10^{-3} s^{-1}–293 K (20 °C) test after 2000 cycles seemingly exhibits secondary cyclic hardening behavior. However, this effect is probably not due to the material deformation response since there is already an obvious influence of the presence of fatigue cracks on the deformation response after 2000 cycles.[16,32] This effect is also observed for other testing conditions, which is coincident with the start of a significant divergence of apparent *E* moduli during reverse loading from compressive and tensile peak stresses.[31,32]).

each TEM foil (about five images were made for dislocation density measurement). The dislocation density was determined from TEM images under multi-beam diffraction conditions with magnifications as low as possible (normally at magnifications from 3300× to 6000×) to increase the statistical significance. Relative comparisons of dislocation microstructures were always made for the same electron-beam direction. Dislocation structure evolution for specific testing conditions was determined by examining samples obtained from an as-received (solution treated) specimen and from test pieces pre-fatigued to selected cycles corresponding to different stages of fatigue life (*e.g.*, Figure 3(a)). Since there was only a slight increase in the dislocation density with increasing cycle number for the ±0.25 pct condition, in particular, considering the scatter in observed dislocation densities, measurements were not made for this condition.

III. EXPERIMENTAL RESULTS

A. *Cyclic Deformation Behavior*

1. *General*

The material exhibits a complex behavior during cyclic loading at both temperatures: firstly cyclic hardening, followed by cyclic softening, and finally by an almost stabilized response phase [for all tests at 293 K (20 °C) and ±0.7 pct at 573 K (300 °C)] or secondary hardening [for ±0.25 and ±0.4 pct tests at 573 K (300 °C)] before failure. The main differences in the cyclic deformation response of the material at 573 K (300 °C) compared to that at 293 K (20 °C) are as follows: firstly, flow stress is serrated at 573 K (300 °C), but not at 293 K (20 °C); secondly, the strain rate sensitivity of cyclic deformation response is positive at 293 K (20 °C), but negative at 573 K (300 °C); thirdly, the hardening rate of the first cyclic hardening phase is higher than that at room temperature; and fourthly, there is a secondary hardening phase at 573 K (300 °C) which occurs for lower strain amplitude conditions (*i.e.*, ±0.4 and ±0.25 pct).[5,9,12,16,17,31,32]

2. *Evolution of Internal Stresses at 293 K and 573 K (20 °C and 300 °C)*

The evolution of effective and back stresses during cyclic loading is shown in Figure 3. Values of the effective stress after the first three quarter cycle are quite similar for the same temperature irrespective of the strain amplitude, while they are very different for different temperatures (Figure 3a). This means that the effective stress is strongly dependent on temperature. However, the temperature dependence of the back stress is much lower. This is due to the short-range interaction of dislocations being strongly influenced by thermal activation, while the temperature does not play an influential role on the long-range interaction of dislocations.[34] The rates of change of maximum stress, back stress, and effective stress are used to quantitatively characterize the evolution of internal stresses, which are given in Table II. The rates of change of back stress during the primary cyclic hardening and softening response stages are much greater than those of effective stress, indicating that the variation in back stress is

Table II. The Rates of Change of Maximum Stress, Back Stress, and Effective Stress During Cyclic Hardening and Cyclic Softening

	$\frac{\frac{d\sigma_{max}}{d(\log N)}}{\frac{dX}{d(\log N)}\Big\vert\frac{d\sigma_E}{d(\log N)}}$		
Conditions	Cyclic Hardening	Cyclic Softening	Secondary Cyclic Hardening
±0.7 pct 10^{-3} s^{-1} 293 K (20 °C)	$\frac{60.1\pm2.5}{54.5\pm2.4\vert3.7\pm2.3}$	$\frac{-20.4\pm0.4}{-19.3\pm4.1\vert-1.4\pm4.1}$	not applicable
±0.7 pct 10^{-3} s^{-1} 573 K (300 °C)	$\frac{107.6\pm1.5}{89.1\pm5.1\vert13.7\pm4.7}$	$\frac{-40.4\pm0.2}{-26.2\pm0.9\vert-13.9\pm0.8}$	
±0.4 pct 10^{-3} s^{-1} 293 K (20 °C)	$\frac{31.3\pm0.6}{25.4\pm2.3\vert4.8\pm2.0}$	$\frac{-19.9\pm0.1}{-14.0\pm0.4\vert-6.3\pm0.4}$	
±0.4 pct 10^{-3} s^{-1} 573 K (300 °C)	$\frac{51.4\pm0.3}{37.4\pm1.0\vert10.7\pm1.4}$	$\frac{-25.0\pm0.5}{-18.0\pm1.9\vert-9.8\pm1.3}$	$\frac{4.3\pm0.8}{4.5\pm2.5\vert7.3\pm0.8}$
±0.25 pct 10^{-3} s^{-1} 293 K (20 °C)	$\frac{9.5\pm1.1}{8.1\pm2.5\vert2.8\pm2.7}$	$\frac{-12.0\pm0.2}{-6.4\pm0.9\vert-6.1\pm0.9}$	not applicable
±0.25 pct 10^{-3} s^{-1} 573 K (300 °C)	$\frac{22.5\pm0.2}{16.4\pm2.4\vert5.3\pm2.2}$	$\frac{-8.4\pm0.6}{-5.0\pm6.1\vert-4.3\pm7.3}$	$\frac{16.3\pm0.3}{4.1\pm2.1\vert13.0\pm2.2}$

Table III. Relative Ratios of the Rate of Change of Effective Stress and of Back Stress to That of Maximum Stress

	$\frac{\left(\frac{d\sigma_E^p}{d(\log N)}\right)}{\left(\frac{d\sigma_{max}^p}{d(\log N)}\right)}$	$\frac{\left(\frac{dX^p}{d(\log N)}\right)}{\left(\frac{d\sigma_{max}^p}{d(\log N)}\right)}$	$\frac{\left(\frac{d\sigma_E^{sof}}{d(\log N)}\right)}{\left(\frac{d\sigma_{max}^{sof}}{d(\log N)}\right)}$	$\frac{\left(\frac{dX^{sof}}{d(\log N)}\right)}{\left(\frac{d\sigma_{max}^{sof}}{d(\log N)}\right)}$	$\frac{\left(\frac{d\sigma_E^{se}}{d(\log N)}\right)}{\left(\frac{d\sigma_{max}^{se}}{d(\log N)}\right)}$	$\frac{\left(\frac{dX^{se}}{d(\log N)}\right)}{\left(\frac{d\sigma_{max}^{se}}{d(\log N)}\right)}$
±0.7 pct 293 K (20 °C)	0.06	0.91	0.07	0.95	not applicable	not applicable
±0.7 pct 573 K (300 °C)	0.13	0.83	0.07	0.95		
±0.4 pct 293 K (20 °C)	0.16	0.81	0.32	0.70		
±0.4 pct 573 K (300 °C)	0.21	0.73	0.39	0.72	1.70	1.05
±0.25 pct 293 K (20 °C)	0.28	0.85	0.51	0.53	not applicable	not applicable
±0.25 pct 573 K (300 °C)	0.24	0.73	0.51	0.60	0.80	0.25

mainly responsible for changes in the cyclic deformation response of the material.

Moreover, the rates of change of effective and back stresses are both higher for 573 K (300 °C) (Figure 3 and Table II). Differences in relative ratios for the rates of change of effective stress between 293 K and 573 K (20 °C and 300 °C) are, however, much higher than those of back stress (Table II). This indicates that the differences in cyclic deformation responses for the material at 293 K and 573 K (20 °C and 300 °C) largely result from changes in effective stress. In particular, the rate of change of effective stress is interestingly much larger than that of back stress during secondary cyclic hardening at 573 K (300 °C) (Table II). In other words, secondary cyclic hardening at 573 K (300 °C) is mainly governed by the effective stress.

3. *Amplitude dependence of the role of internal stresses*

The relative ratios of effective stress (or back stress) to maximum stress are given in Table III in order to indicate how internal stresses influence the cyclic deformation response when strain amplitude changes. Lowering imposed plastic strain amplitude; the relative ratio increases for effective stress, while decreasing for the back stress. This indicates that the contribution of effective stress to the material cyclic response increasingly becomes greater for lower strain amplitudes. In contrast, back stress becomes less influential on cyclic deformation response for lower strain amplitude conditions.

B. *Microstructure*

1. *Microstructural evolution during cyclic loading at 293 K (20 °C)*

a. Cyclic hardening response stage. In the as-received condition, dislocations are mainly present in the form of planar structures, *e.g.*, regular arrays of dislocations, stacking faults, *etc*. At the beginning of cyclic loading, grain-to-grain misorientations inducing plastic strain incompatibilities between grains result in a significant increase in the number of dislocations close to the grain boundaries to preserve the continuity of material (Figures 4(a) and (b)). This means that to accommodate inhomogeneously distributed plastic deformation from grain to grain, numerous dislocations necessarily need to

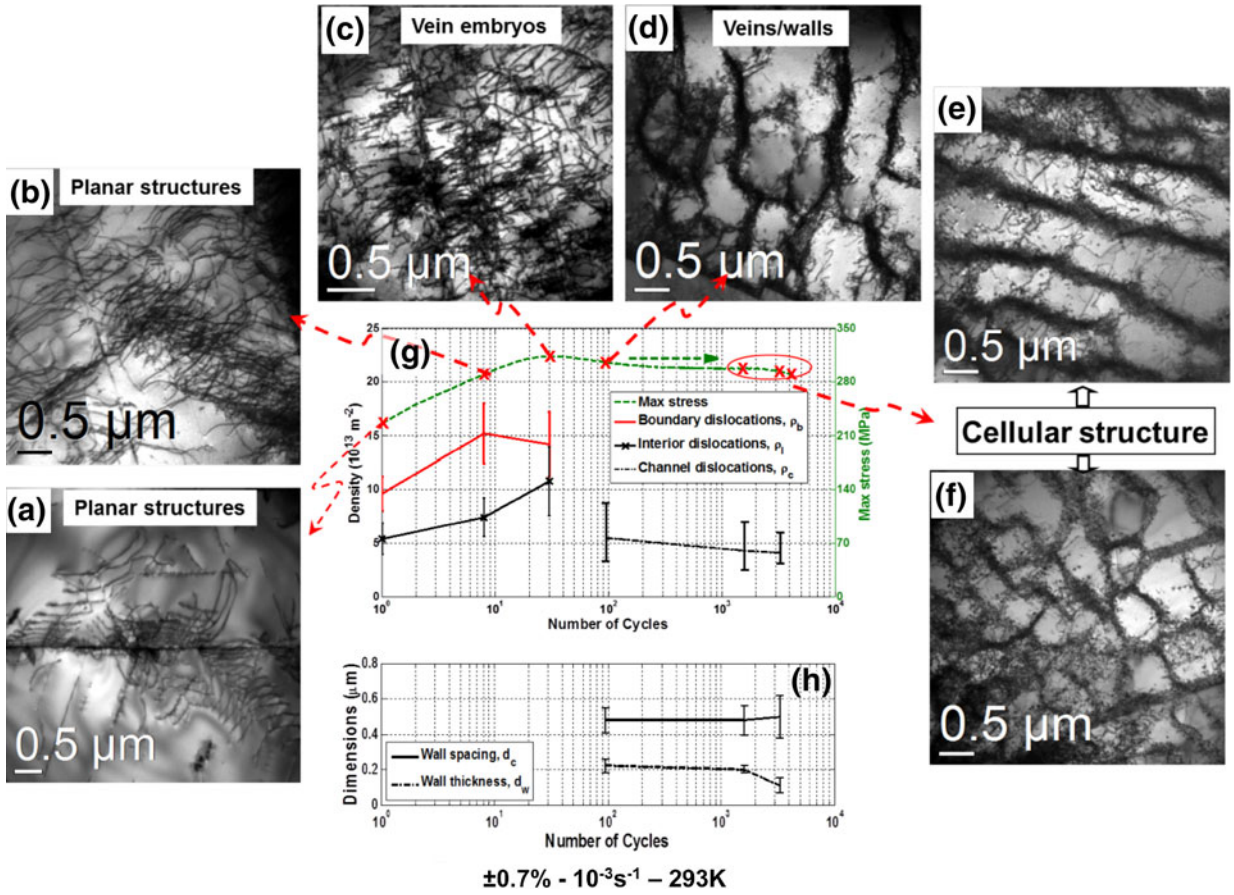

Fig. 4—Dislocation evolution and the corresponding cyclic deformation behavior of AISI 316L steel for the ±0.7 pct–10^{-3} s^{-1}–293 K (20 °C) test. (*a*) through (*f*) the development of dislocations from planar to cellular structures.

be generated as explained by Ashby.[20] In contrast, dislocations inside grains also increase in their number, but with a lower rate. These observations provide a motivation to differentiate and quantify the evolution of dislocation densities both in regions adjacent to grain boundaries and inside grains, in order to understand their relationship with internal stresses during cyclic loading (refer to Section IV–A–1). The quantification of dislocation densities is given in Figure 4(g). After a number of cycles, dislocations are distributed more homogeneously within the grains (Figures 4(c) and (g)).

b. Cyclic softening and stabilized (or secondary cyclic hardening) response stages. The grain-to-grain plastic strain incompatibilities are relieved thanks to the activity of secondary slip (including cross slip) upon further loading (Figure 4(c)). Secondary slip activity promotes dislocation interactions, resulting in (1) an increase in the annihilation rate of dislocations, leading to a slight decrease in dislocation density, and (2) the rearrangement of dislocations to form lower and more stable energetic configurations, *i.e.*, dislocation high/low density regions (Figures 4(d) through (f) and 5(a) through (c)). The number of dislocations in low density regions slightly decreases with the number of cycles (Figure 4(g)). The width of dislocation high density regions also decreases during cyclic loading, *i.e.*, dislocations within walls become denser upon further loading (Figure 4(h)). The dislocation arrangements to dislocation high/low density regions contribute to the further relief of the grain-to-grain strain incompatibilities. It, however, raises other strain incompatibilities between dislocation high/low density regions on a finer scale, *i.e.*, at the intragranular scale. Finally, the stabilized condition of these strain incompatibilities is established upon further loading once dislocations seek their most stable configuration for a given testing condition. In the stabilized condition, both wall dislocations and channel dislocations attain their saturation value. The channel dislocations can move back and forth during cyclic loading in the stabilized stage.

2. *Microstructural evolution during cyclic loading at 573 K (300 °C)*

There are some similarities in the microstructural evolution of the material during cyclic loading at 573 K and 293 K (300 °C and 20 °C), such as (1) an increase in dislocation density during the first cycles (Figures 6(a), (b), and 7(a)) and (2) the rearrangement of dislocations to form dislocation high/low density structures toward the end of fatigue life (Figures 6(c) through (e)).

There are distinct differences in dislocation evolution behavior at these two temperatures:

(a) The incidence of point defects at 573 K (300 °C) is much more profuse than at room temperature

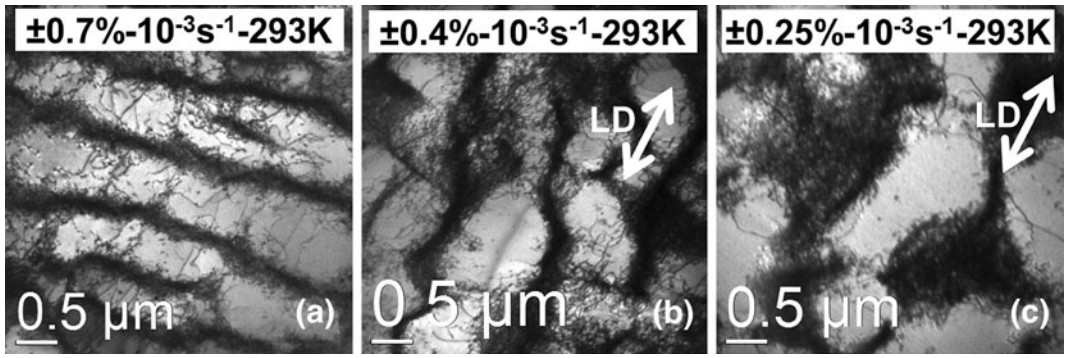

Fig. 5—Microstructural condition at the end of life with reducing strain amplitude. (*a*) Well-organized dislocation walls for the ±0.7 pct–10^{-3} s^{-1}-293 K (20 °C) test. (*b*) Less well-organized dislocation walls for the ±0.4 pct–10^{-3} s^{-1}–293 K (20 °C) test. (*c*) Dislocation carpet-like structure for the ±0.25 pct–10^{-3} s^{-1}–293 K (20 °C) test.

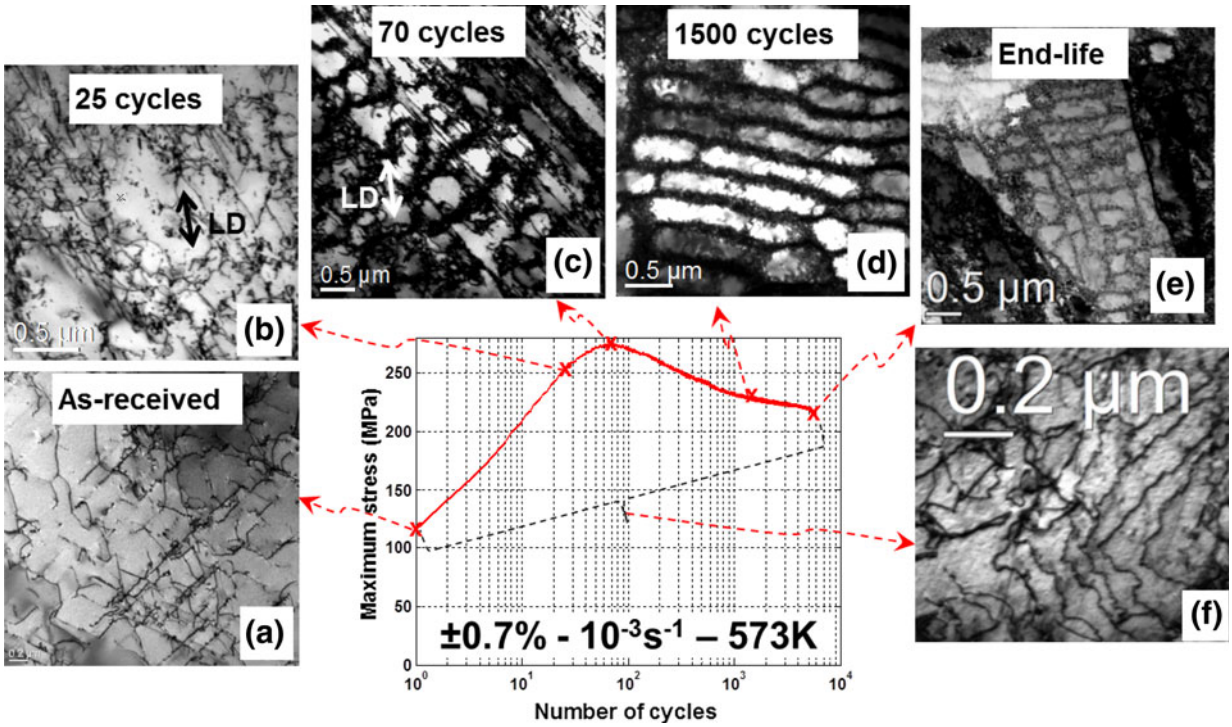

Fig. 6—(*a*) through (*f*) Dislocation evolution and its corresponding cyclic deformation behavior in AISI 316L steel at ±0.7 pct–10^{-3} s^{-1}–573 K.

(Figure 8(a)). These point defects are mainly of the vacancy type because there is a preponderance of vacancy-type dipoles[35] and probably also because of the lower energy of formation for vacancies than for interstitials.[36] Vacancies promote the diffusion of solute atoms (C and N), leading to the formation of solute atom atmospheres around dislocation cores which can restrict the movement of dislocations.[18,37] This results in more zigzag dislocation lines (Figures 6(f) and 8(b)).

(b) Higher numbers of dislocations are generated during cyclic hardening (Figure 7(a)) and a smaller wall spacing exists toward the end of life at 573 K (300 °C) (Figure 7(b)).

(c) A striking feature observed at 573 K (300 °C) is a corduroy structure {which is often found within localized deformation bands of well-aligned tiny point defects along certain orientations [Figures 8(c) and (d)]}. This feature is not only seen in irradiated materials[38] but was also observed in the same material cyclically loaded in vacuum without any irradiation damage by Gerland.[11,39] The generation of corduroy structure in laboratory air was observed for the first time by the authors of this present study.[9] This microstructure is believed to be responsible for the secondary cyclic hardening of AISI 316L during cyclic loading in the dynamic strain aging regime.[9,11]

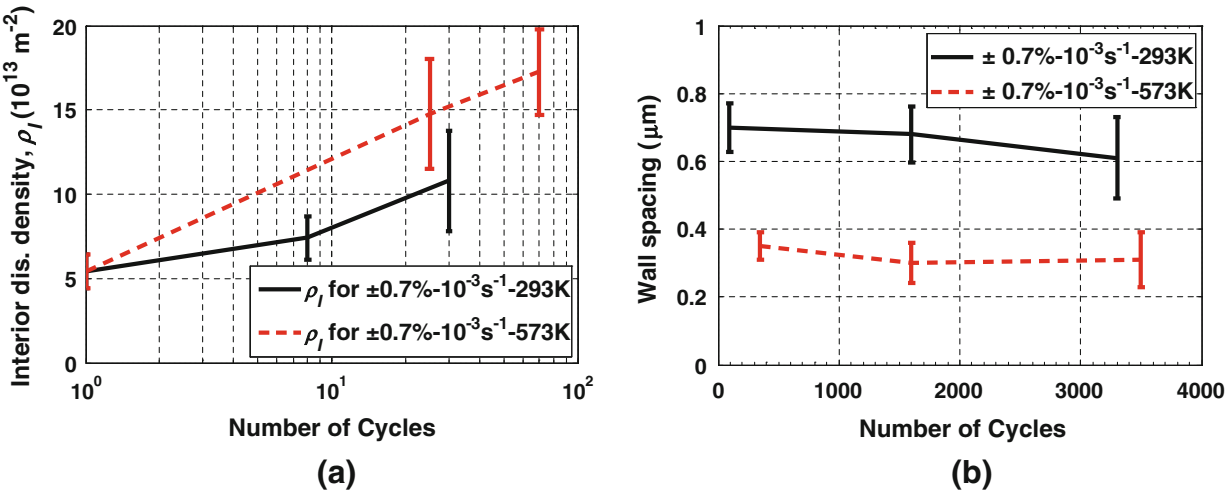

Fig. 7—(*a*) Interior dislocation densities and (*b*) dislocation wall spacing for the ±0.7 pct conditions at 293 K and 573 K (20 °C and 300 °C).

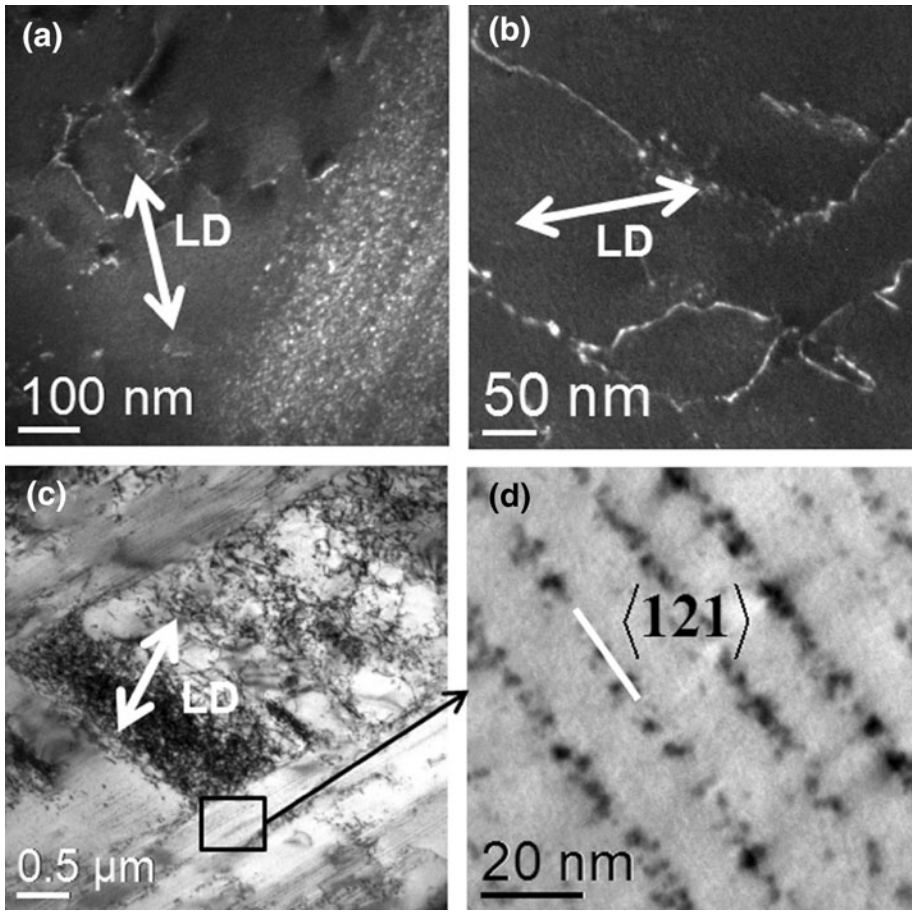

Fig. 8—(*a*) The presence of profuse vacancies which are mainly present within localized deformation bands. (*b*) Dislocations are pinned by solute atoms. (*c*, *d*) Localized deformation bands within which there is a corduroy structure.

3. *Amplitude dependence*

During cyclic hardening response, dislocations are less dense for lower strain amplitude tests (*e.g.*, Figure 9), resulting in smaller rates of primary cyclic hardening (Table II).

The configuration of dislocation high/low density regions is strongly dependent on imposed plastic strain. Toward the end of life, dislocation configuration exhibits a stronger tendency to planar character and is less well organized for lower strain amplitude conditions

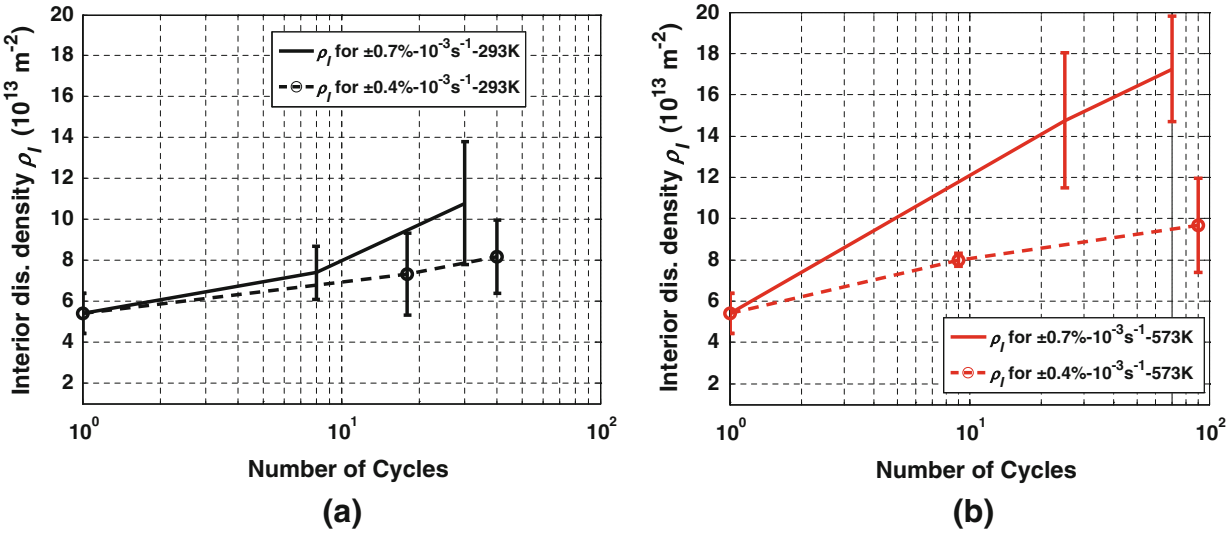

Fig. 9—The evolution of the interior dislocation density for ±0.7 pct–10^{-3} s^{-1} (solid lines) and for ±0.4 pct–10^{-3} s^{-1} (dashed lines) at (*a*) 293 K (20 °C) and (*b*) 573 K (300 °C).

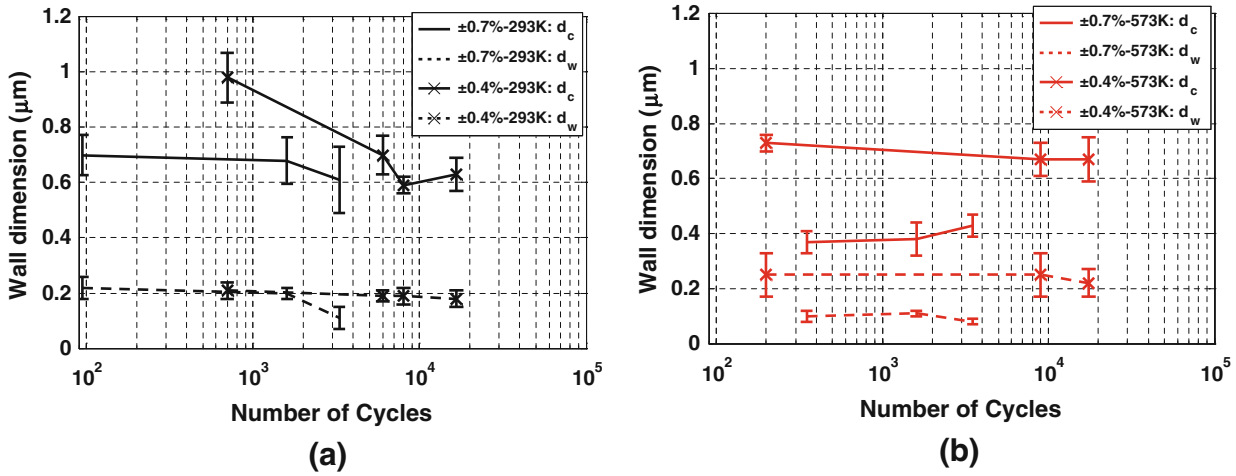

Fig. 10—Dislocation wall dimension (*a*) at 293 K (20 °C) and (*b*) 573 K (300 °C): spacing and thickness for the ±0.4 (lines with symbols) and ±0.7 pct (lines without symbols).

(Figure 5). The degree of dislocation configuration organization can be quantitatively characterized by the wall-to-wall spacing and wall thickness for the ±0.4 and ±0.7 pct conditions (Figure 10). This clearly shows that for lower strain amplitudes, (1) dislocation walls are further apart and (2) dislocation wall thickness is wider and wall dislocation density is lower.

IV. DISCUSSION

A. *History Dependence of the Relationship Between Back Stress and Dislocation Microstructure*

1. *Cyclic hardening response stage*

Due to inhomogeneous plastic deformation between grains (Figure 11(a)), dislocation densities close to grain boundaries are significantly higher (Figure 4(g)) in order to preserve grain-to-grain continuity.[20,40] These dislocations are often referred to as geometrically necessary dislocations (GNDs), although the term is not restricted only to those dislocations necessary to accommodate the geometrical change of features subjected to plastic deformation.[20,22] Such dislocations are present in the form of pile-ups adjacent to grain boundaries (Figures 4(b) and 11(b)) and are associated with intergranular back stress (X_{inter}). A significant increase in the density of these dislocations (ρ_b) results in a rapid rise in this back stress. During plastic deformation, the interior dislocation density (ρ_I) also increases, but at a slower rate (Figure 4(g)), reducing the gradient of dislocation density between regions close to grain boundaries and regions inside grains, *i.e.*, lessening the grain-to-grain strain incompatibility. Moreover, secondary slip activity on the one hand relieves the grain-to-grain plastic strain incompatibility and on the other hand results in the

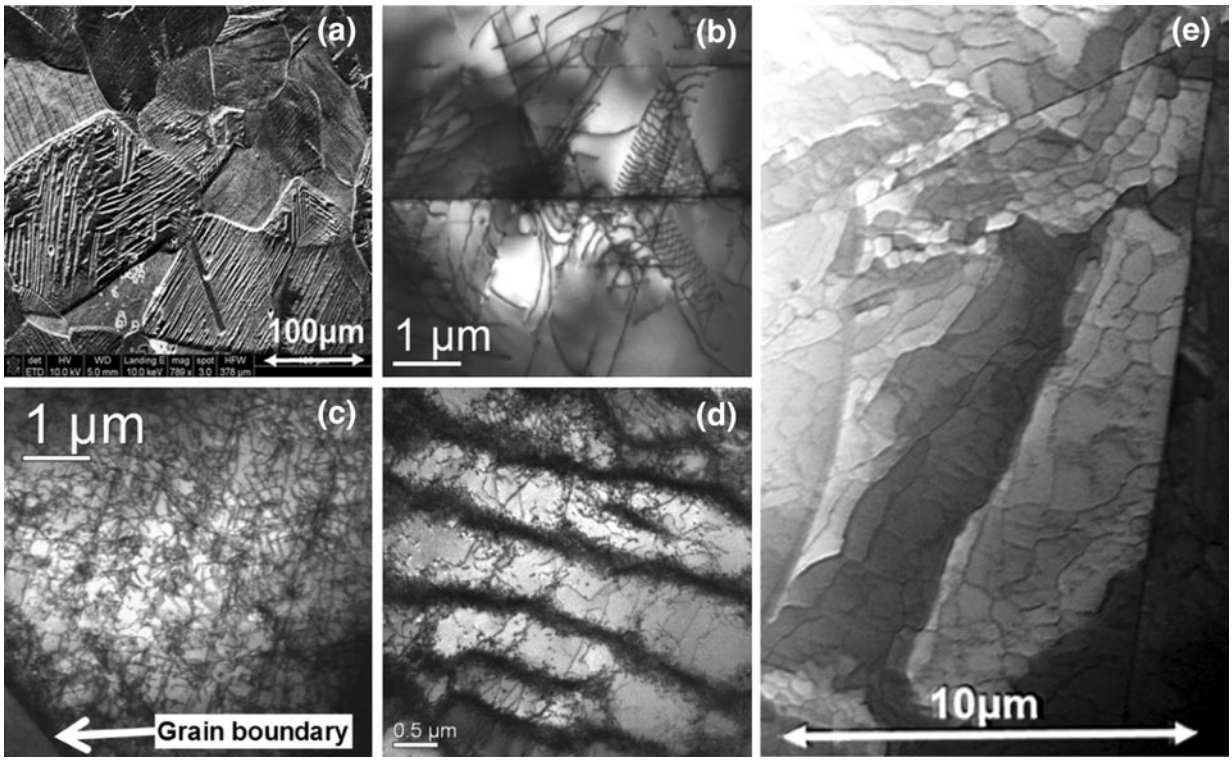

Fig. 11—(*a*) Grain-to-grain plastic strain incompatibilities, (*b*) dislocation pile-ups close to a grain boundary, (*c*) strong activity of secondary slip and a homogeneous distribution of dislocations over a grain, (*d*) dislocation walls and channels, and (*e*) the fragmentation of grains into different groups of cellular structure in order to accommodate the plastic strain incompatibilities.

abundance of interior dislocations, leading to a more homogeneous distribution of dislocations over grains (Figures 4(c) and 11(c)). Consequently, X_{inter} is proportional to the difference in the development of boundary dislocations and interior dislocations during primary cyclic hardening, *i.e.*,

$$2X_{\text{inter}} \propto f_{\text{b}}\left(\sqrt{\rho_{\text{b}}} - \sqrt{\rho_{\text{I}}}\right) \qquad [1]$$

with f_{b} being a proportionality coefficient which is found to intimately relate to the area fraction occupied by boundary dislocations.[12]

Different types of dislocation groups (which are present due to inhomogeneous plastic deformation between phases of different strength levels) can be related to corresponding internal stresses by means of the Taylor relationship.[14,41,42] In other words, a given internal stress (σ_i) can then relate to a specific type of dislocation (ρ_i) by the Taylor-like relationship:

$$\sigma_i = M\alpha Gb\sqrt{\rho_i}, \qquad [2]$$

where M is the average Taylor factor.

2. *Cyclic softening and stabilized response stages*

Once interior dislocations become abundant and occupy a much larger area fraction than boundary dislocations, dislocations strongly rearrange to form dislocation high/low density regions and finally to form their most stable configuration under a given condition. In addition, the slip activity and the rearrangement of dislocations also contribute to the process of grain fragmentation to a greater extent (Figure 11(e)). Grain fragmentation and the formation of dislocation high/low density regions have two effects:

(a) They contribute to relief of the intergranular back stress X_{inter} until the requirement of material continuity between grains is completely fulfilled by the response of collective fragmented volumes (Figure 11(e)). This indicates that X_{inter} achieves its stable value after a high number of cycles once dislocation structures are well formed. At this condition, X_{inter} is associated with dislocations of GND type [named stabilized intergranular GNDs ($\rho^{\text{sat}}_{\text{GNDs}-\text{inter}}$)]. These GNDs are the minimum required number of dislocations to accommodate the grain-to-grain plastic strain incompatibility at the stabilized condition and are present mainly in regions close to boundaries of fragmented volumes. In conjunction with the relationship between X_{inter} and dislocation condition during primary cyclic hardening (Eq. [1]), the evolution of X_{inter} during cyclic loading can consequently be expressed by

$$2X_{\text{inter}} \propto \left[f_{\text{b}} \times \left(\sqrt{\rho_{\text{b}}} - \sqrt{\rho_{\text{I}}}\right) + \sqrt{\rho^{\text{sat}}_{\text{GNDs}-\text{inter}}}\right] \qquad [3]$$

(b) On a finer scale, *i.e.*, an intragranular scale, the rearrangement of dislocations creates other strain incompatibilities between dislocation high/low density regions,[43] *e.g.*, dislocation walls and channels

(Figure 11(d)). Consequently, the intragranular back stress X_{inter} increases with the development of these fine dislocation structures until the most stable structures form. As a result, X_{inter} evolves with another type of GND ($\rho_{GNDs\text{-}intra}$) which is present in the interface between dislocation high/low density regions. It is worth noting that the back stress associated with this type of GND is proportional to the difference between the square root density of dislocations within walls (named wall dislocations, ρ_w) and within channels (called channel dislocations, ρ_c), and the fraction of walls (f_w).[14,41,44] Therefore, the intragranular back stress arising due to the formation of dislocation wall/channel structures during cyclic loading ($2X_{inter}$) can be described as follows according to Mughrabi's composite model[14]:

$$2X_{intra} \propto \left(\sqrt{\rho_w} - \sqrt{\rho_c}\right) \times f_w \qquad [4]$$

Once the stabilized condition of material response is established, the requirement of material continuity is totally fulfilled both at the intergranular scale and the intragranular scale (Figure 12). A minimum quantity of dislocations is required to move back and forth in dislocation low density regions to accommodate the imposed plastic strain during cyclic loading.

The strongly intermittent slip manner of dislocation motion due to the locking effect of solute atom atmospheres makes the relief of strain incompatibilities more difficult at 573 K (300 °C), causing a more rapid increase in the intergranular back stress. In addition, solute atom atmospheres effectively lock dislocations, resulting in higher numbers of dislocations for cyclic loading at 573 K (300 °C) than for the equivalent conditions at 293 K (20 °C) (Figures 7(a) and 9). Moreover, the cell dimension depends on total dislocation density.[45,46] This explains why the diameter of dislocation cells at 573 K (300 °C) is smaller than for the equivalent conditions at 293 K (20 °C) as shown in Figures 7(b) and 10. Although thermal activation lowers the absolute value of back stress, a faster development of dislocation microstructures into well-organized configurations results in a more rapid increase in the intragranular back stress at 573 K (300 °C). Consequently, the rate of change of back stress at 573 K (300 °C) is higher than for the equivalent conditions at 293 K (20 °C) (Table II).

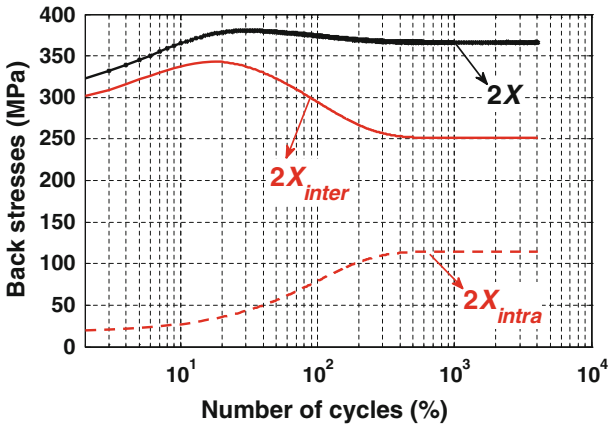

Fig. 12—The evolution of back stresses during cyclic loading for the ±0.7 pct–10^{-3} s^{-1}–293 K (20 °C) test condition.

B. *History Dependence of the Relationship Between Effective Stress and Dislocation Microstructures*

The increase in dislocation density results in more frequent short-range interactions of dislocations with themselves and with point defects. In particular, when secondary slip is strongly active, Lomer–Cottrell, Hirth, collinear, and coplanar interactions of individual dislocations in FCC materials[33,47–49] result in the formation of sessile/glissile dislocation junctions (Figure 13), leading to an increase in effective stress. Since dislocation junctions form due to the activity of secondary slip relating to the increase in interior dislocations, the increment of effective stress ($\sigma_E^{R(d)}$) due to the interactions between dislocations with themselves is proportional to $\sqrt{\rho_I}$, *i.e.*, $\sigma_E^{R(d)} \propto \sqrt{\rho_I}$.

The strong short-range dislocation interaction with solute atoms, and later in life with corduroy structure, however, induces a significant increase in effective stress (Table II), causing the more noticeable primary cyclic hardening and in particular the secondary cyclic hardening response. The short-range dislocation interaction with solute atoms leads first to the formation of Suzuki atmospheres in faulted areas of partial dislocations and relatively later in life to the formation of short-range ordered Snoek atmospheres.[9] The significant increase in effective stress during the primary cyclic hardening response results from the locking effectiveness of Suzuki atmospheres. Screw dislocations, however, can more easily escape from solute atom atmospheres under sufficient stress when the activation energy for cross slip is lowered due to the formation of dislocation junctions.[50,51] During primary cyclic hardening, a high number of dislocation junctions form, leading to easier cross slip of screw dislocations, which strongly weakens the locking effect of Suzuki atmospheres.[9] Moreover, the strong activity of cross slip also results in an increase in the annihilation rate of screw dislocations, finally leading to a decrease in the density of these dislocations. The weakened locking effect of Suzuki atmosphere and the decrease in screw dislocations during cyclic softening make the effective stress decrease, in particular for the ±0.7 pct–10^{-3} 1/s–573 K (300 °C) test condition (Figure 3(a)). This decrease in the effective stress is, however, not high for lower strain amplitudes at 573 K (300 °C) because it is quickly compensated for by the development of the corduroy structure (Figure 8(d)) which very effectively locks dislocations.[9] Since the locking effectiveness of solute atom atmospheres results in a higher immobile dislocation density during primary cyclic hardening (Figure 9), the contribution of the strong interaction between dislocations and solute atoms to the additional increment of the effective stress can be accommodated by the following expression, $\sqrt{\left(\frac{C_s}{C_{s,0}}\right)\rho_I}$,

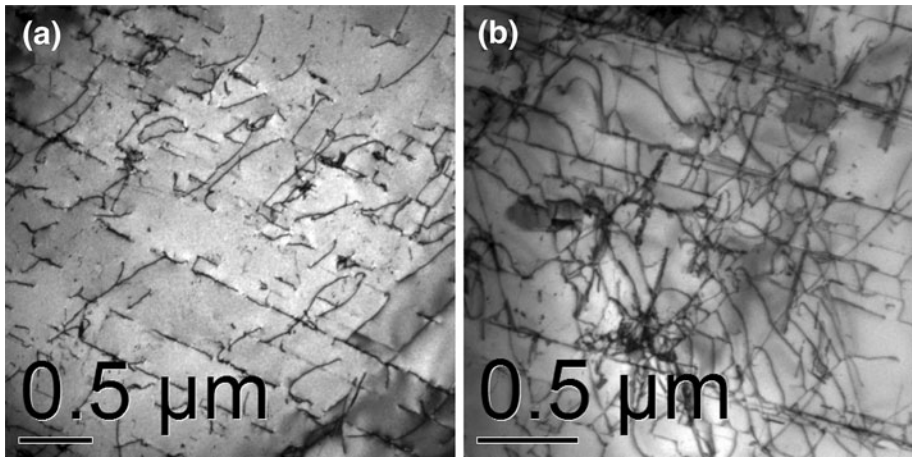

Fig. 13—Short-range dislocation–dislocation interactions. Sessile dislocation junctions (straight segment junctions of dislocations) when the total dislocation density is about (*a*) 8×10^{13} 1/m^2 and (*b*) 11.8×10^{13} 1/m^2.

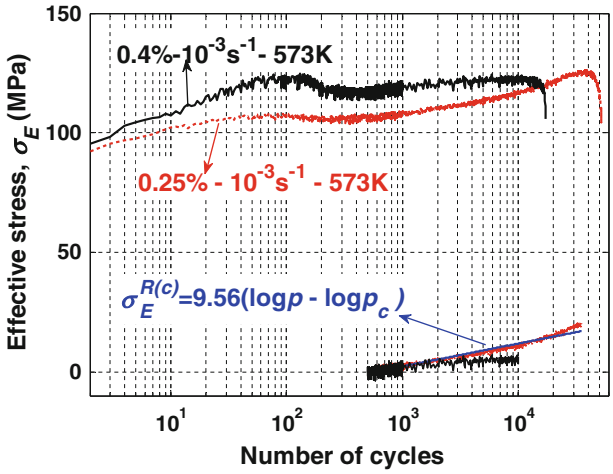

Fig. 14—The evolution of effective stress at 573 K (300 °C) for ±0.25 and ±0.4 pct conditions.

where $C_{s,0}$ and C_s are the nominal concentration and the saturation concentration, respectively, of solute atom s along dislocation lines.[52]

The corduroy structure continuously develops after a high number of cycles, resulting in considerable increase in the effective stress. This is mainly responsible for the secondary cyclic hardening. The secondary cycle hardening phase is observed for both the ±0.25 and ±0.4 pct conditions. The rates of additional increase in the effective stress during the beginning of this cyclic response stage are the same for both loading cases (Figure 14). The earlier presence of fatigue cracks for the ±0.4 pct test, however, interferes with the macroscopic manifestation of the change in the effective stress. If fatigue cracks were not formed earlier for the ±0.4 pct test, the apparent rate of change of effective stress for this condition would be similar to that of the ±0.25 pct condition. The model of the evolution of effective stress associating with the development of the corduroy structure is therefore made based on the observed increase in $\sigma_E(\log p)$ for the ±0.25 pct condition. Fitting the increment of effective stress with respect to p gives

$$2\sigma_E^{R(c)} = 9.56\{\log p - \log p_c\},$$

where the MacCauley bracket $\{x\} = \begin{cases} x & \text{if } x \geq 0 \\ 0 & \text{if } x < 0. \end{cases}$

p_c is the plastic strain accumulated to form the well-developed corduroy structure. The accumulated plastic strain p_c is strain amplitude dependent. The lower the strain amplitude, the earlier the formation of the well-organized corduroy structure.

C. *Strain Amplitude Dependence of the Relationship Between Microstructure and Internal Stresses*

It is important to remember that for lower strain amplitude conditions, (1) fewer dislocations are generated (Figure 9), (2) the planar structure of dislocations persists to a higher life fraction, and (3) less organized dislocation structures form toward the end of life. Because smaller imposed plastic strains induce lower grain-to-grain plastic strain incompatibility, the intergranular back stress is correspondingly less for lower strain amplitudes. Moreover, the quantity of well-organized dislocation configurations is less for lower strain amplitudes toward the end of life (Figure 10), *i.e.*, dislocation walls have lower strength with reducing strain amplitude. Consequently, the intragranular back stress becomes smaller for lower strain amplitudes.

The decrease in intragranular back stress with reducing strain amplitude is, however, not only due to the degree of good organization of dislocation structures toward the end of fatigue life but also depends on the character of dislocation configuration. Small imposed plastic strain results in a slight change in the dislocation number during cyclic loading, resulting in very mobile dislocations for well-annealed FCC materials. Dislocations therefore tend to form the lowest energetic configuration, a structure close to the equilibrium state,[53,54] which is associated with negligible long-range stress fields. In contrast, for high imposed strain

conditions, dislocations are dense and move in an intermittent manner (*e.g.*, avalanche motion of dislocations such as PSBs which are active for higher strain amplitudes, *e.g.*, the ±0.4 and ±0.7 pct conditions), to form a self-organized dislocation structure (SODS). The SODS is a non-equilibrium thermodynamic configuration and is associated with long-range stress fields.[55,56] In other words, intragranular back stresses (arising during plastic deformation for which dislocation movement is prone to be planar and be less intermittent in character) are much smaller than those of high imposed strain for which dislocation motion tends to be wavy. This explains why

(a) At higher strain amplitudes for which well-organized dislocation walls/channels form, the influence of back stress on the cyclic deformation response far outweighs that of effective stress.
(b) In contrast, at lower strain amplitudes (*e.g.*, ±0.25 pct) for which dislocation structures form with the lowest energetic configuration, effective stress becomes more influential in the material cyclic response.

At 573 K (300 °C), dislocations move in a more planar way. However, dislocation density is higher (Figure 9), resulting in more well-organized dislocation structures toward the end of life (Figure 10). Moreover, the movement of dislocations is very intermittent due to the locking effect of solute atoms. Consequently, the rate of increase of intergranular back stress is higher than for the equivalent conditions at 293 K (20 °C).

V. CONCLUDING REMARKS

Effective stress is associated with the short-range ordering interactions of dislocations with themselves and with point defects. The activity of secondary slip results in the formation of dislocation junctions at an early stage of plastic deformation, leading to the increase in effective stress. The additional strong short-range dislocation interactions at 573 K (300 °C), initially with solute atoms, and later in life with corduroy structure, cause a significant increase in effective stress which is responsible for the more noticeable primary cyclic hardening and secondary cyclic hardening response.

Back stresses are long-range stresses associated with the presence of collective dislocations over different length scales. At the grain-to-grain scale, intergranular back stress increases with the number of dislocation pile-ups which are present close to grain boundaries to accommodate the plastic strain incompatibilities between grains at the beginning of cyclic loading. Upon further loading, the strong activity of secondary slip results in higher numbers of dislocations inside grains, *i.e.*, dislocations are distributed more homogeneously over grains, relieving the intergranular back stress. In other words, intergranular back stress relates to differences in the numbers of dislocations close to grain boundaries and within the grains. Once interior dislocations become abundant, dislocations start strongly rearranging to form dislocation high/low density regions and seek to form their most stable configuration. This process of rearrangement on the one hand contributes to further relief of the intergranular back stress, but on the other hand raises the intragranular back stress on a smaller scale due to the formation of dislocation high/low density regions (*e.g.*, walls and channels). When the stabilized condition of dislocation microstructures is established, the requirement of material continuity is totally fulfilled both at the intergranular and intragranular scales, leading to the saturation values of these back stresses. For high strain amplitudes where dislocations tend to move more quickly in a wavy way, the back stresses are mainly responsible for the change in cyclic deformation response. In contrast, lower imposed strain amplitudes encourage effective stress to play a more important role on cyclic deformation response, while lessening the influence of back stresses.

ACKNOWLEDGMENTS

The financial support by the Swiss Competence Centre for Materials Science and Technology (CCMX-MERU), ABB Turbo-Generators, ALSTOM (Switzerland), and Swissnuclear is gratefully acknowledged. We would also like to express our appreciation to our colleagues Dr Koen G.F. Janssens of the Paul Scherrer Institute in Switzerland for his help with provision of the AISI 316L pipe steel and Jan Lukas Eurich for his support with dislocation density measurement. The contributions of Dr. Rolf Erni and Daniel Schreier of the Electron Microscopy Centre (ZEM) of EMPA are also duly acknowledged.

NOMENCLATURE

AISI	American Iron and Steel Institute (Material Grading Systems)
D_g, d_w, and d_c	Grain size, dislocation wall thickness, and dislocation cell size (*i.e.*, channel width), respectively
FCC	Face-centered cubic
f_w	Area fraction of dislocation walls
E, G	Elastic modulus, shear modulus, respectively
GNDs	Geometrically necessary dislocations
LD	Loading direction
N	Number of cycles
PSBs	Persistent slip bands
p and p_c	Accumulated plastic strain and the plastic strain accumulated to form the well-developed corduroy structure, respectively

SODS	Self-organized dislocation structure
TEM	Transmission electron microscope
X, X_{inter}, and X_{intra}	Back stress, intergranular back stress, and intragranular back stress, respectively
ρ_t, ρ_b, ρ_I, ρ_w, and ρ_c	The densities of total dislocations, of dislocations close to grain boundaries, of dislocation within the grains, of dislocations within walls, and of dislocations in channels, respectively
$\rho_{\text{GNDs-inter}}$ and $\rho_{\text{GNDs-intra}}$	Densities of GNDs required to accommodate the plastic strain incompatibility between grains and between dislocation high/low density regions, respectively
$\sigma_{\max}$ and σ_0	Maximum stress of every cycle and yield stress, respectively
σ_E, σ_E^0, σ_E^R; $\sigma_E^{R(d)}$, and $\sigma_E^{R(c)}$	Effective stress, initial effective stress, the increment of effective stress; the increment of effective stress due to interactions between dislocations with themselves, and with a corduroy structure, respectively

REFERENCES

1. J.C. Grosskreutz and M. Mughrabi: *Constitutive Equations in Plasticity*, A.S. Argon, ed., MIT Press, Cambridge, 1975, pp. 251–326.
2. H. Mughrabi: *Fatigue*, 2010, vol. 2010 (2), pp. 3–26.
3. C.E. Feltner and C. Laird: *Acta Metall.*, 1967, vol. 15, pp. 1621–32.
4. C.E. Feltner and C. Laird: *Acta Metall.*, 1967, vol. 15, pp. 1633–53.
5. M.S. Pham, C. Solenthaler, K.G.F. Janssens, and S.R. Holdsworth: *Mater. Sci. Eng. A Struct.*, 2011, vol. 528, pp. 3261–69.
6. M. Gerland, J. Mendez, P. Violan, and B.A. Saadi: *Mater. Sci. Eng., A*, 1989, vol. 118, pp. 83–95.
7. Y.F. Li and C. Laird: *Mater. Sci. Eng., A*, 1994, vol. 186, pp. 87–103.
8. J. Polak, K. Obrtlik, and M. Hajek: *Fatigue Fract. Eng. Mater. Struct.*, 1994, vol. 17, pp. 773–82.
9. M.S. Pham and S.R. Holdsworth: *Mater. Sci. Eng., A*, 2012, vol. 556, pp. 122–33.
10. M. Gerland, R. Alain, B.A. Saadi, and J. Mendez: *Mater. Sci. Eng., A*, 1997, vol. 229, pp. 68–86.
11. M. Gerland and P. Violan: *Mater. Sci. Eng.*, 1986, vol. 84, pp. 23–33.
12. M.S. Pham, S.R. Holdsworth, K.G.F. Janssens, and E. Mazza: *Int. J. Plasticity*, 2013, vol. 47, pp. 143–64.
13. D. Kuhlmann-Wilsdorf and C. Laird: *Mater. Sci. Eng.*, 1979, vol. 37, pp. 111–20.
14. H. Mughrabi: *Acta Metall.*, 1983, vol. 31, pp. 1367–79.
15. X. Feaugas: *Acta Metall.*, 1999, vol. 47, pp. 3617–32.
16. M.S. Pham and S.R. Holdsworth: *Procedia Eng.*, 2011, vol. 10, pp. 1069–74.
17. M.S. Pham and S.R. Holdsworth: in *The 8th European Solids Mechanics Conference*, Graz, Austria, 2012.
18. A. Cottrell: *Dislocations and Plastic Flow in Crystals*, Clarendon Press, Oxford, 1953.
19. X. Feaugas and C. Gaudin: *Mater. Sci. Eng. A Struct.*, 2001, vol. 309, pp. 382–85.
20. M.F. Ashby: *Philos. Mag.*, 1970, vol. 21, pp. 399–424.
21. N. Hansen: *Metall. Mater. Trans. A*, 2001, vol. 32A, pp. 2917–35.
22. H. Mughrabi: *Philos. Mag.*, 2006, vol. 86, pp. 4037–54.
23. D. Kuhlmann-Wilsdorf and C. Laird: *Mater. Sci. Eng.*, 1979, vol. 37, pp. 111–20.
24. A. Abel and Y.S. Chung: *Scripta Metall.*, 1979, vol. 13, pp. 907–10.
25. X. Feaugas: *Recent Res. Dev. Mater. Sci.*, 2003, vol. 4, pp. 35–64.
26. X. Feaugas, S. Catalao, P. Pilvin, and M.T. Cabrillat: *Mater. Sci. Eng. A Struct.*, 2008, vols. 483–484, pp. 422–25.
27. X. Feaugas and P. Pilvin: *Adv. Eng. Mater.*, 2009, vol. 11, pp. 703–09.
28. A.F. Armas, O.R. Bettin, I. Alvarezarmas, and G.H. Rubiolo: *J. Nucl. Mater.*, 1988, vol. 155, pp. 646–49.
29. V.S. Srinivasan, R. Sandhya, K.B.S. Rao, S.L. Mannan, and K.S. Raghavan: *Int. J. Fatigue*, 1991, vol. 13, pp. 471–78.
30. M. Gerland, J. Mendez, J. Lepinoux, and P. Violan: *Mater. Sci. Eng., A*, 1993, vol. 164, pp. 226–29.
31. M.S. Pham: Diss. ETH No. 20864, ETH Zurich, Zurich, 2013, p. 252.
32. M.S. Pham and S.R. Holdsworth: *Int. J. Fatigue*, 2013, vol. 51, pp. 36–48.
33. M.J. Whelan: *Proc. R. Soc. Lond. Ser. A*, 1959, vol. 249, p. 114.
34. U.F. Kocks, A.S. Argon, and M.F. Ashby: *Prog. Mater Sci.*, 1975, vol. 19, pp. 1–281.
35. J.G. Antonopoulos, L.M. Brown, and A.T. Winter: *Philos. Mag.*, 1976, vol. 34, pp. 549–63.
36. W.M. Lomer: *Prog. Met. Phys.*, 1959, vol. 8, pp. 255–320.
37. A.H. Cottrell and B.A. Bilby: *Proc. Phys. Soc. Lond. Sect. A*, 1949, vol. 62, pp. 49–62.
38. D. Caillard, J.L. Martin, and B. Jouffrey: *Acta Metall.*, 1980, vol. 28, pp. 1059–67.
39. M. Gerland, B.A. Saadi, and P. Violan: *Mater. Sci. Eng.*, 1987, vol. 96, pp. L1–L4.
40. N.A. Fleck and J.W. Hutchinson: *Adv. Appl. Mech.*, 1997, vol. 33, pp. 295–361.
41. H. Mughrabi: *Mater. Sci. Eng., A*, 2004, vol. 387, pp. 209–13.
42. Y. Estrin, L.S. Toth, A. Molinari, and Y. Brechet: *Acta Mater.*, 1998, vol. 46, pp. 5509–22.
43. H. Mughrabi: *Phys. Status Solidi A Appl. Res.*, 1987, vol. 104, pp. 107–20.
44. E. Nes: *Prog. Mater Sci.*, 1997, vol. 41, pp. 129–93.
45. D.L. Holt: *J. Appl. Phys.*, 1970, vol. 41, pp. 3197–201.
46. D. Knoesen and S. Kritzinger: *Acta Metall.*, 1982, vol. 30, pp. 1219–22.
47. W.M. Lomer: *Philos. Mag.*, 1951, vol. 42, pp. 1327–31.
48. A.H. Cottrell: *Philos. Mag.*, 1952, vol. 43, pp. 645–47.
49. R. Madec, B. Devincre, L. Kubin, T. Hoc, and D. Rodney: *Science*, 2003, vol. 301, pp. 1879–82.
50. A.N. Stroh: *Proc. Phys. Soc. Lond. Sect. B*, 1954, vol. 67, pp. 427–36.
51. J. Bonneville and B. Escaig: *Acta Metall.*, 1979, vol. 27, pp. 1477–86.
52. J.Y. Cheng, S. Nemat-Nasser, and W.G. Guo: *Mech. Mater.*, 2001, vol. 33, pp. 603–616.
53. D. Kuhlmann-Wilsdorf: *Mater. Sci. Eng. A Struct.*, 1989, vol. 113, pp. 1–41.
54. M. Zaiser: *Mater. Sci. Eng. A Struct.*, 2001, vol. 309, pp. 304–315.
55. M. Glazov, L.M. Llanes, and C. Laird: *Phys. Status Solidi A Appl. Res.*, 1995, vol. 149, pp. 297–321.
56. M. Zaiser and A. Seeger: *Dislocations in Solids*, Elsevier, Amsterdam, 2002.